http://www.imavs.org/

A 3D Rotating Laser Based Navigation Solution for Micro Aerial Vehicles in Dynamic Environments

Hailong Qin[2], Mo Shan[1], Yingcai Bi[2], Jiaxin Li[2],Menglu Lan[2]
F. Lin[1], Y.F. Zhang [3] and Ben M. Chen[2]

***Abstract*— In this article, a 3D rotating laser-based navigation framework for a micro aerial vehicle (MAV) to fly autonomously in the dynamic environment is presented. The proposed navigation framework consists of a 6-degree of freedom (DoF) localization module and a 3D dynamic mapping module. By extracting and aligning 3D point cloud features from a dense point cloud which generates by a self-designed rotating 2D laser setup, we are able to solve the laser distortion issue while estimating the 6-DoF pose of MAV. In addition, the dynamic mapping module could further eliminate the dynamic trail so that a clean dense 3D map can be reconstructed.**

Our proposed navigation framework detects the dynamic target based on the spatial constraints and propagates without dense point cloud clustering. Through filtering the detected dynamic obstacles, the proposed localization approach is proven to be robust to the environment variations.

We demonstrate the utility of our proposed framework in both real indoor environment with highly dynamic obstacles using a customized MAV platform.

I. INTRODUCTION

The applications of MAV on autonomous tasks have been intensively studied [1] [2] [3]. The fundamental requirements for automation of MAV are (1) Onboard sensing capability. The MAV should utilize the onboard sensors such as Laser scanner [4], vision [5]and other sensors (sonar and radar)[6] to obtain the information about an unknown environment. (2) Onboard processing capability. Based on the sensing information, the onboard processor should achieve state estimation for control and environment mapping for planning [7]. (3) Onboard state feedback capability. the state estimation from external sensors should be fused with onboard inertial measurement unit (IMU) or the other sensors for a closed feedback control loop [8]. The above capabilities are critical to the safety navigation of MAV. More importantly, they are in fact interdependent, performance deterioration of single component could degrade the whole autonomous system. We can formalize the mentioned capabilities into sensing, perception(includes state estimation and mapping) and control modules correspondingly.

[1]Mo Shan and F. Lin are with the Temasek Laboratories, National University of Singapore, Singapore. E-mail: {shanmo, tsllinf}@nus.edu.sg

[2]Hailong Qin, Jiaxin Li, Yingcai Bi, Menglu Lan and Ben M. Chen are with the Department of Electrical & Computer Engineering, NUS, Singapore. E-mail: {mpeqh, jli, yingcaibi, lanmenglu, bmchen}@nus.edu.sg

[3]Y.F. Zhang is with the Department of Mechanical Engineering, National University of Singapore, Singapore. E-mail: {mpezyf}@nus.edu.sg

The sensing and perception modules are challenging for MAVs because of the size and computational power constraints. To full fill the autonomous navigation requirements, the following sensor setup is selected in general:

1) Laser, usually known as laser range finder (LRF) is a highly precise active sensor which can provide planarly range measurement to a large range field. Comparing with the passive sensor such as cameras, the laser range finder is still effective in low illumination environment. And the commercial product such as Hokuyo UTM-30LX-EW 2D laser scanner is able to achieve a 30 Hz measurement update which is beneficial to the state estimation. However, the 2D LRF itself cannot measure the 3D environment completely due to the limited vertical measurement [9]. This disadvantage could lead to the failure of MAV autonomous tasks because of the absent of information about the environment for state estimation and obstacle avoidance.
2) Camera, either monocular or multiple camera system is considered as an alternative to the active LRF sensor. The camera system is low in both weight and power consumption makes it promising to the MAV platform. And the camera system is a natural 3D sensing device which full of texture and color information [10]. Yet, the information from camera system is still insufficient to the MAV platform in certain conditions such as illumination variation and low texture environment [11].

Regarding the execution of autonomous task of MAVs, the key requisite is to locate itself in a GPS-denied environment. Moreover, the obstacles should be reliably detected in real time to generate an obstacle-free path for flying [12]. However, it is still challenging to achieve these requirements by the previously mentioned sensor setup individually. Therefore, a combination of these two sensors [13]or the RGBD camera [14]is proposed. Among all the proposed solutions, the vision-based approach is selected as the basic module in the algorithm which still could not resolve the illumination issue [15].

Beyond the sensor setup choice, the perception module is not longer dealing with the static environment alone. Traditionally, the basic assumption for the simultaneous localization and mapping (SLAM) is the static environment due to the reason that the current map measurement should be registered into previous global map. The realistic condition includes a lot of moving target which could confuse the

http://www.imavs.org/

perception algorithm. Even though the vision based approach could reject the moving target in the motion estimation phase through iterative process [16]. However, this approach is not very effective to the slow moving target. In addition, this process is computationally expensive. To the whole autonomous system, the moving target could degrade the performance in following conditions: (1) If the perception module still works (can estimate the ego-motion of MAVs), then the map cannot update properly in the dynamic environments and leave dynamic trails [17]. The dynamic trails could further affect the planning since the obstacles cannot be properly detected. (2) The worst condition is the failure of perception module because of the environment is no longer static, the ego motion of MAVs could not be estimated anymore. Burgard et al. [18] propose to differentiate the dynamic and static cells in 2D grid map by evaluating the expectation maximization. This approach is straightforward to extend to 3D but expensive in computation due to the ray-tracing.

In this article, we present a complete customized and integrated system consisting of a MAV platform with onboard processor, a rotating laser-based localization module and a dynamic mapping module. The MAV platform could provide onboard computation and flying capability. The localization module could utilize the continuous rotating laser scans to achieve a high frequency motion estimation update. And the dynamic mapping module could detect and eliminate the moving target for both localization and further real-time mapping. The developed techniques allow for reliable motions estimation and efficient dynamic map update. The robustness of the proposed framework is evaluated in multiple dynamic environments.

II. RELATED WORKS

The demanding of MAVs to fly autonomously in typical GPS-denied environments such as indoor and forest are rapidly growing. Based on the different platforms and sensors for perception, several research groups have carried out some demonstrations for practical applications. Stephan Weiss et al. [7] use an MAV from ASL and onboard monocular camera together with IMU achieved a flight height of $70m$. However, in contrast to our work this computationally constrained solution could not handle the 3D navigation properly since that the obstacle cannot be reliably detected from sparse points. Similarly, Forster et al. [19] use same sensor setup but a semi-dense image registration approach. The proposed approach for MAV high altitude fly shows that the motion estimation of UAV can be efficient and robust through pixel intensity based alignment. However, computational expensive dense mapping module is required for a complete 3D navigation [20]. To observe the points depth directly, some groups utilize the stereo camera [21]. However, this approach could fail in low feature or texture environment. The RGBD camera is well-suited for the MAVs' indoor navigation task which measures the depth from projecting infrared pattern [2]. Comparing with passive camera systems, the infrared pattern can estimate the depth on the textureless condition such as the white wall. Yet the view field of the infrared pattern is limited which could cause problems when the obstacles are out of MAV view field. To cope with this issue, it is straightforward for the MAVs to equip with multiple RGBD cameras. However, the computational cost rises correspondingly.

The laser-based state estimation technologies are largely adopted by unmanned ground vehicle (UGV). For instance, the utilization of 2D LRF on UAV and small size UGV - Hector SLAM which estimates the 2D motion [22]. Together with the height measurement, a 3D Octomap can be constructed for obstacle detection. However, this approach relies on the reliable and fast height measurement or else will result in an inconsistent 3D map. Similar to this approach, Morris et al. [23] utilize the sparse visual features together with the 2D LRF for motion estimation. Yet, it is still not a direct 3D measurement. In contrast to this approach, our motor driving 2D LRF can directly measure the depth of 3D environment.

Different from 2D LRF, the 3D LRF could provide an accurate 3D dense range measurement regardless of the illumination variation. The sensing capability of 3D LRF makes it possible for UGVs to detect obstacles in all directions [17]. Combined with camera systems for state estimation, the sensing and perception modules are robust and effective. Considering the size and weight limitations, the 3D LDFs are rarely utilized on UAVs. Besides that, the power consumption of 3D LRF could lead to the reduction of endurance.

A combination of visual for localization and laser for obstacle detection is considered as a good choice: Either monocular camera or stereo camera can provide an 6 DoF so that the state estimation is not limited to 2D planner space. Based on the state estimation information, either the static or rotating LRF can construct a 3D map. A similar approach is proposed by Cover et al. [15] use vision for localization and laser for obstacle detection. However, this combination could not work in dark environment and obstacles out of view.

Similar to our approach, Hovermap [24] utilizes a continuous rotating laser on a Micro Aerial Vehicle for state estimation and mapping. However, the GPS signal is fused for a better motion estimation. And more importantly, scenario with moving target is not considered. Matthias et al. [4] build a MAV platform with the camera system for odometry and rotating laser to detect obstacles. Similar to vision-based approach, illumination variation and textureless cause the failure of motion estimation.

The other important issue is dynamic map update. Hahnel et al. [25] consider the moving target as outliers and removed. Yet, this approach is not a correct representation of the map at each time instant due to the lack of moving target. Similar strategy has adopted by [26] [27].

III. SYSTEM CONFIGURATION

The MAV platform is designed by NUS UAV Group with the capability of wind resistance and heavy payload. The platform has a 128 cm tip to tip length and a maximum take-off weight with the 2 kg payload. A self-designed power distributor module provides multiple power sources including 3.3 V, 5 V and 12 V for on-board electronics. The on-board

http://www.imavs.org/

flight controller is Pixhawk with customized flight control algorithms. For the mission control computer, we use the Intel-NUC board. The powerful NUC board equipped with a 5th Generation Intel Core i7-5557U processor. The optimized size is and the optimized weight is only 200 g including a cooling fan. The platform is shown in Fig. 1.

Fig. 1: MAV platform.

IV. TERMINOLOGY AND NOTATION

In this article, we define the body frame of UAV platform as U and local laser coordinate as L. For the rotating laser device, one rotation of the laser range finder is from -90° to 90° in CW or 90° to -90° in CCW as denoted (θ) in Fig. 2 while the x-y plane is the 0° planar plane. Thus for kth rotation, the laser coordinate is expressed as L_k. The global coordinate is O. For a single laser point $p(x,y,z)$ in kth rotation, the coordinate is expressed as $X^U_{k,l,p}$, $X^L_{k,l,p}$ and $X^O_{k,l,p}$ correspondingly.

Fig. 2: Rotating angle illustration in front view and isometric view.

V. ALGORITHM OVERVIEW

In this article, a sensing and a perception modules for MAV in dynamic environments are presented. The proposed algorithm contains following components:

- Feature extraction and alignment: extract the defined feature from 2D laser scan and align the scans in 3D point cloud sequence.
- Motion estimation: estimate the motion based on the optimization of feature alignment error metric.
- dynamic mapping: update the 3D map for dense mapping and motion estimation refinement.

The following section will describe the above components in detail.

VI. FEATURE EXTRACTION AND FEATURE ALIGNMENT

To solve the motion estimation problem efficiently, we select the feature points $p(x,y,z)$ in each scan instead of all the points to build the correspondence between neighbouring scans. The natural properties of laser scan in real environment is large amounts of data, noisy and contains of outliers which makes the feature extraction quite difficult as described by Abdul [28] . In their work, outlier rejection and robust fitting is applied to extract reliable feature from point cloud. For 2D laser scan, variation of a scanning point in a local neighborhood is used to select the feature point. For a point p in a single scan l of kth rotation, the average length of the edges $l_{avg,p}$ incident to it in a local neighborhood:

$$l_{avg,p} = \frac{1}{N} \sum_{q \varepsilon N(i)} ||X^L_{k,l,p} - X^L_{k,l,q}|| \tag{1}$$

Where N stands for total number of points adjacent to p and q stands for the neighbor point of p. A relative variation ratio $R_{k,l,p}$ is defined to select edge point $e_{k,l,i}$(with a variation ratio larger than threshold) or flat point $f_{k,l,i}$ (with a variation ratio smaller than threshold).

$$R_{k,l,p} = \frac{l_{avg}}{||X^L_{k,l,p}||} \tag{2}$$

In our work, since we have extracted feature points as edge points and flat points, two Euclidean distance based relationship will be built accordingly to associate the feature points in different rotations.

- To a edge point p in kth rotation, we can search for the nearest neighbor point of p, m in $(k+1)th$ rotation from the beginning of $(k+1)th$ rotation through reprojection. In order to build a point to line correspondence, we further search for a neighbor point of m in consecutive scan and denote it as n. We can calculate the distance from the edge point p to its corresponding line by the following equation:

$$d_e = \frac{|v_l \times v_e|}{|v_l|} \tag{3}$$

  Where v_l stands for $(X^L_{k+1,l,m} - X^L_{k+1,l,n})$ and v_e stands for $(X^L_{k,l,p} - X^L_{k+1,l,m})$ as shown in Fig. 6.
- To a flat point q in kth rotation, we need to search for the nearest neighbor point of q, r in $(k+1)th$ through reprojection. After that, another two neighbor points of r, s and t need to be searched so that three non-collinear points can construct a plane. The objective is to minimize the distance from the flat point q to its corresponding plane. The unit normal of plane can be calculated as :

$$n = \frac{v_{p1} \times v_{p2}}{|v_{p1} \times v_{p2}|} \tag{4}$$

Where v_{p1} is $(X^L_{k+1,l,s} - X^L_{k+1,l,r})$ and v_{p2} is $(X^L_{k+1,l,t} - X^L_{k+1,l,r})$. The distance from flat point q to its corresponding plane can be calculated as

$$d_p = n \cdot v_p \tag{5}$$

where v_p stands for $(X^L_{k,l,q} - X^L_{k,l,r})$.

VII. MOTION ESTIMATION

Translation and rotation of a 3D point p in $(k+1)th$ rotation $X^L_{k+1,l,p}$ with respect to last laser frame L_k is expressed by,

$$X_{k,l,p} = \widehat{X^L_{k+1,l,p}} = R^k_{k+1} X^L_{k+1,l,p} + P^k_{k+1} \tag{6}$$

Where

$$R^k_{k+1} = \begin{bmatrix} 1 & 0 & 0 \\ 0 & c\alpha & -s\alpha \\ 0 & s\alpha & c\alpha \end{bmatrix} \begin{bmatrix} c\beta & 0 & s\beta \\ 0 & 1 & 0 \\ -s\beta & 0 & c\beta \end{bmatrix} \begin{bmatrix} c\gamma & -s\gamma & 0 \\ s\gamma & c\gamma & 0 \\ 0 & 0 & 1 \end{bmatrix}$$

$$P^k_{k+1} = \begin{bmatrix} p_x \\ p_y \\ p_z \end{bmatrix}$$

α, β and γ are the UAV body Euler angle correspondingly. Based on the transformation relationship$T^k_{k+1} = (R^k_{k+1}, P^k_{k+1})$.We can further express the transformation relationship as a nonlinear function f,

$$f(X^L_{k+1,l,p}) = X_{k,l,p} \tag{7}$$

Consider the point to line correspondence in equation (3). To estimate the motion between $(k+1)th$ rotation and kth rotation, we need to minimize the distance d_e to 0 as described in following function.

$$d_e = w_1(f(X_{k+1,l,m}), f(X_{k+1,l,n})) \to 0 \tag{8}$$

Similarly, the point to plane distance d_p can be expressed by,

$$d_p = w_2(X^L_{k,l,q}), f(X_{k+1,l,r}), f(X_{k+1,l,s}), f(X_{k+1,l,t})) \to 0 \tag{9}$$

Through combining the feature point correspondence, we can build a nonlinear function $w(T^k_{k+1}) = d$ to express (8) and (9). Therefore, the square error function can be established as

$$S = (w(T^k_{k+1}))^2 \tag{10}$$

Since the objective value of $w(T^k_{k+1})$ is 0. To minimize the objective function, mainly two methods can be adopted for real time application, Levenberg-Marquardt(LM) [29] method and Trust-Region-Reflective method (TRR)[30]. Compared with the LM approach, TRR is more accurate and less costly when the incrementally updated result is far away from solution. The update step $\sigma_i = (T^k_{k+1})_{i+1} - (T^k_{k+1})_i$ can be obtained by solving

$$\min_{\sigma \in N} \psi_i(\sigma) \tag{11}$$

$$s.t. \|\sigma\|_2 \leq \Delta_k \tag{12}$$

Where $\psi_i(\sigma) = g^T\sigma + \frac{1}{2}\sigma^T H \sigma$ and g and H are the gradient and Hessian, respectively of w evaluated at $(T^{k+1}_k)_i$ and $\Delta_k > 0$ is the trust region radius. We can further define the acceptable ratio by

$$r_k = \frac{(\psi(0) - \psi_i(\sigma_i))}{(w(T^k_{k+1}) - w(T^k_{k+1} + \sigma_i))} \tag{13}$$

Which is used to decide the iteration of trial step σ_i.

VIII. DYNAMIC MAPPING

The safety of autonomous navigation of MAVs requests the 3D map updating with dynamic obstacles detection. Once when the dynamic obstacles are properly detected and removed, the perception module could perform a good localization based on the static objects. In the proposed framework, an efficient structure is kept for dense 3D map so that it could maintain a consistent dense representation in long term. In this article, we only discuss the 3D map without dynamic objects for perception.

The fundamental assumption to identify the dynamic objects is the consistency of visibility: in the continuously updating environment, if a point along the laser ray is visually blocked by a point that we previously observed, then the previously point could be further considered as dynamic moving target. Instead of directly adopting the ray-tracing for visibility validation [31], the point cloud representation for the map is utilized to ensure a smooth information flow. Moreover, the spherical coordinates representation is introduced to represent the geometrical information. The usage of spherical coordinate allows to store the depth of point in a 2D distance map format [32] so that the dynamic obstacles can be efficiently detected. To a point *p(x,y,z)* in one point cloud set, its corresponding spherical coordinate form is

$$\rho = \sqrt{x^2 + y^2 + z^2} \tag{14}$$

$$\theta = atan2(y, x) \tag{15}$$

$$\phi = arccos(\frac{z}{\rho}) \tag{16}$$

To a point cloud set which generated by the kth rotating of laser V^o_k in global coordinate, its associated spherical coordinate form is V^s_k. Initially, we assume that most of the points in V^s_k are static. The spatial difference between a point $X^s_{k+1,l,p}$ and $X^s_{k,l,p}$ is calculated by

$$\left\| X^s_{k+1,l,p} - X^s_{k,l,p} \right\| \tag{17}$$

The spatial difference serves to distinguish between the dynamic points and static points. Moreover, the angle between $X^s_{k+1,l,p}$ and upcoming new point in local spherical coordinate could further propagate the knowledge on the points. The greater the angle difference, the less the previous knowledge changed. Through this approach, the dynamic points are removed so that the motion could be correctly updated. The whole localization and dynamic mapping workflow can be described by Fig. 3.

http://www.imavs.org/

http://www.imavs.org/

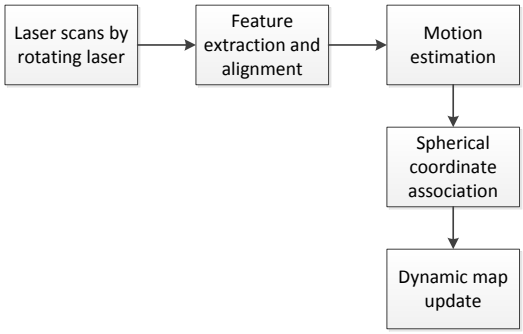

Fig. 3: System workflow.

IX. EXPERIMENTAL RESULTS

The proposed framework is verified in the real environment directly instead of simulated environments to show the robustness and efficiency of the solution. In the designed experiment, the MAV has a maximum flying speed of $1.5m/s$ in clustered indoor corridor. The onboard stereo camera is setup for online visualization of the scene.

A. Flying in corridor environment

This experiment is designed to verify the accuracy of the motion estimation module and mapping module without dynamic obstacles. Since the ground truth of the motion estimation is not available, the accuracy of the motion estimation is evaluated by the reconstructed environment. For instance, the vertical wall should keep upright. The result is shown in Fig. 4.

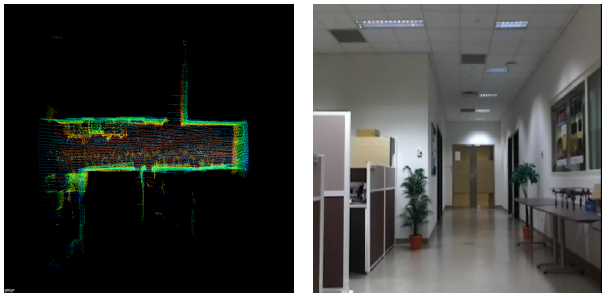

(a) (b)

Fig. 4: Reconstructed corridor environment.

From the reconstructed environment we can see that the accuracy of motion estimation is good since the reconstructed environment well represented real condition.

B. Hovering with dynamic obstacles

This experiment is designed to test the dynamic module specifically. The MAV is controlled by the information from the motion estimation module in the presence of moving obstacles. The failure of the map updating could lead to the dynamic trails as shown in Fig. 5. Based on the experiment result, the dynamic mapping module removes the continuous moving obstacle(target in black rectangle) successfully and keeps a static map for further motion estimation refinement as shown in Fig. 6 .

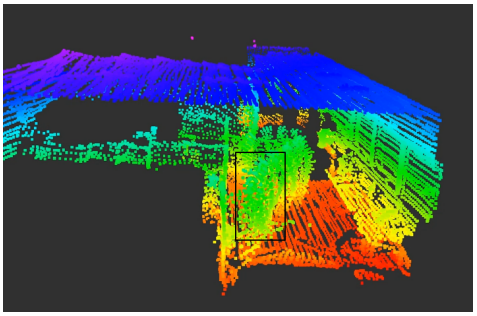

Fig. 5: Moving obstacles caused dynamic trails.

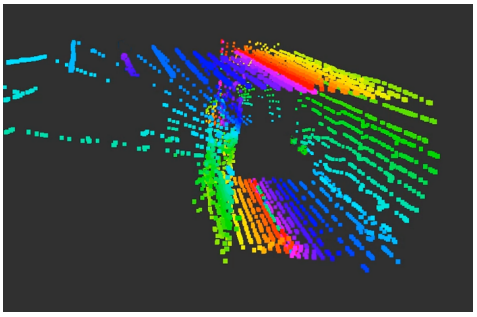

Fig. 6: Dynamic obstacles filtering.

X. CONCLUSION

In this article, we present a novel rotating laser based motion estimation and dynamic mapping framework to achieve MAV autonomous navigation in a GPS-denied environment. The proposed framework solves the laser distortion issue by feature-based motion estimation and dynamic trails through by point based filtering instead of voxel grid based ray-tracing. Further, we show the accuracy and robustness of our proposed framework in the experiments. The rotating laser based framework estimates the ego-motion of MAV while filtering the dynamic obstacles successfully.

REFERENCES

[1] S. Shen, N. Michael, and V. Kumar, "Autonomous multi-floor indoor navigation with a computationally constrained mav," in *Robotics and automation (ICRA), 2011 IEEE international conference on*. IEEE, 2011, pp. 20–25.

[2] A. S. Huang, A. Bachrach, P. Henry, M. Krainin, D. Maturana, D. Fox, and N. Roy, "Visual odometry and mapping for autonomous flight using an rgb-d camera," in *International Symposium on Robotics Research (ISRR)*, vol. 2, 2011.

[3] L. Heng, L. Meier, P. Tanskanen, F. Fraundorfer, and M. Pollefeys, "Autonomous obstacle avoidance and maneuvering on a vision-guided mav using on-board processing," in *Robotics and automation (ICRA), 2011 IEEE international conference on*. IEEE, 2011, pp. 2472–2477.

[4] M. Nieuwenhuisen, D. Droeschel, M. Beul, and S. Behnke, "Autonomous navigation for micro aerial vehicles in complex gnss-denied environments," *Journal of Intelligent & Robotic Systems*, pp. 1–18, 2015.

[5] M. Blösch, S. Weiss, D. Scaramuzza, and R. Siegwart, "Vision based mav navigation in unknown and unstructured environments," in *Robotics and automation (ICRA), 2010 IEEE international conference on*. IEEE, 2010, pp. 21–28.

[6] J. Müller and W. Burgard, "Efficient probabilistic localization for autonomous indoor airships using sonar, air flow, and imu sensors," *Advanced Robotics*, vol. 27, no. 9, pp. 711–724, 2013.

[7] S. Weiss, M. W. Achtelik, S. Lynen, M. Chli, and R. Siegwart, "Real-time onboard visual-inertial state estimation and self-calibration of mavs in unknown environments," in *Robotics and Automation (ICRA), 2012 IEEE International Conference on*. IEEE, 2012, pp. 957–964.

[8] L. Meier, P. Tanskanen, L. Heng, G. H. Lee, F. Fraundorfer, and M. Pollefeys, "Pixhawk: A micro aerial vehicle design for autonomous flight using onboard computer vision," *Autonomous Robots*, vol. 33, no. 1-2, pp. 21–39, 2012.

[9] S. Kohlbrecher, J. Meyer, T. Graber, K. Petersen, U. Klingauf, and O. von Stryk, "Hector open source modules for autonomous mapping and navigation with rescue robots," in *Robot Soccer World Cup*. Springer, 2013, pp. 624–631.

[10] F. Fraundorfer, L. Heng, D. Honegger, G. H. Lee, L. Meier, P. Tanskanen, and M. Pollefeys, "Vision-based autonomous mapping and exploration using a quadrotor mav," in *2012 IEEE/RSJ International Conference on Intelligent Robots and Systems*. IEEE, 2012, pp. 4557–4564.

[11] S. Yang, S. A. Scherer, K. Schauwecker, and A. Zell, "Onboard monocular vision for landing of an mav on a landing site specified by a single reference image," in *Unmanned Aircraft Systems (ICUAS), 2013 International Conference on*. IEEE, 2013, pp. 318–325.

[12] S. Lai, K. Wang, H. Qin, J. Q. Cui, and B. M. Chen, "A robust online path planning approach in cluttered environments for micro rotorcraft drones," *Control Theory and Technology*, vol. 14, no. 1, pp. 83–96, 2016.

[13] J. Zhang and S. Singh, "Visual-lidar odometry and mapping: Low-drift, robust, and fast," in *2015 IEEE International Conference on Robotics and Automation (ICRA)*. IEEE, 2015, pp. 2174–2181.

[14] J. Zhang, M. Kaess, and S. Singh, "Real-time depth enhanced monocular odometry," in *2014 IEEE/RSJ International Conference on Intelligent Robots and Systems*. IEEE, 2014, pp. 4973–4980.

[15] S. Scherer, J. Rehder, S. Achar, H. Cover, A. Chambers, S. Nuske, and S. Singh, "River mapping from a flying robot: state estimation, river detection, and obstacle mapping," *Autonomous Robots*, vol. 33, no. 1-2, pp. 189–214, 2012.

[16] R. Mur-Artal, J. Montiel, and J. D. Tardós, "Orb-slam: a versatile and accurate monocular slam system," *IEEE Transactions on Robotics*, vol. 31, no. 5, pp. 1147–1163, 2015.

[17] F. Pomerleau, P. Krüsi, F. Colas, P. Furgale, and R. Siegwart, "Long-term 3d map maintenance in dynamic environments," in *2014 IEEE International Conference on Robotics and Automation (ICRA)*. IEEE, 2014, pp. 3712–3719.

[18] W. Burgard, C. Stachniss, and D. Hähnel, "Mobile robot map learning from range data in dynamic environments," in *Autonomous Navigation in Dynamic Environments*. Springer, 2007, pp. 3–28.

[19] C. Forster, M. Pizzoli, and D. Scaramuzza, "Svo: Fast semi-direct monocular visual odometry," in *Robotics and Automation (ICRA), 2014 IEEE International Conference on*. IEEE, 2014, pp. 15–22.

[20] M. Pizzoli, C. Forster, and D. Scaramuzza, "Remode: Probabilistic, monocular dense reconstruction in real time," in *2014 IEEE International Conference on Robotics and Automation (ICRA)*. IEEE, 2014, pp. 2609–2616.

[21] C. De Wagter, S. Tijmons, B. D. Remes, and G. C. de Croon, "Autonomous flight of a 20-gram flapping wing mav with a 4-gram onboard stereo vision system," in *2014 IEEE International Conference on Robotics and Automation (ICRA)*. IEEE, 2014, pp. 4982–4987.

[22] S. Kohlbrecher, O. Von Stryk, J. Meyer, and U. Klingauf, "A flexible and scalable slam system with full 3d motion estimation," in *Safety, Security, and Rescue Robotics (SSRR), 2011 IEEE International Symposium on*. IEEE, 2011, pp. 155–160.

[23] W. Morris, I. Dryanovski, J. Xiao, *et al.*, "3d indoor mapping for micro-uavs using hybrid range finders and multi-volume occupancy grids," in *In RSS 2010 workshop on RGB-D: Advanced Reasoning with Depth Cameras*. Citeseer, 2010.

[24] L. Kaul, R. Zlot, and M. Bosse, "Continuous-time three-dimensional mapping for micro aerial vehicles with a passively actuated rotating laser scanner," *Journal of Field Robotics*, vol. 33, no. 1, pp. 103–132, 2016.

[25] D. Hahnel, R. Triebel, W. Burgard, and S. Thrun, "Map building with mobile robots in dynamic environments," in *Robotics and Automation, 2003. Proceedings. ICRA'03. IEEE International Conference on*, vol. 2. IEEE, 2003, pp. 1557–1563.

[26] D. Hähnel, D. Schulz, and W. Burgard, "Mobile robot mapping in populated environments," *Advanced Robotics*, vol. 17, no. 7, pp. 579–597, 2003.

[27] D. F. Wolf and G. S. Sukhatme, "Mobile robot simultaneous localization and mapping in dynamic environments," *Autonomous Robots*, vol. 19, no. 1, pp. 53–65, 2005.

[28] A. Nurunnabi, G. West, and D. Belton, "Robust methods for feature extraction from mobile laser scanning 3d point clouds."

[29] S. Roweis, "Levenberg-marquardt optimization," *Notes, University Of Toronto*, 1996.

[30] Y.-x. Yuan, "A review of trust region algorithms for optimization," in *ICIAM*, vol. 99, 2000, pp. 271–282.

[31] F. Ferri, M. Gianni, M. Menna, and F. Pirri, "Dynamic obstacles detection and 3d map updating," in *Intelligent Robots and Systems (IROS), 2015 IEEE/RSJ International Conference on*. IEEE, 2015, pp. 5694–5699.

[32] P. Gohl, D. Honegger, S. Omari, M. Achtelik, M. Pollefeys, and R. Siegwart, "Omnidirectional visual obstacle detection using embedded fpga," in *Intelligent Robots and Systems (IROS), 2015 IEEE/RSJ International Conference on*. IEEE, 2015, pp. 3938–3943.

http://www.imavs.org/